



# Composition, architecture and biomechanical properties of articular cartilage in differently loaded areas of the equine stifle

Maria Fugazzola<sup>1</sup>  | Mikko T. Nissinen<sup>2</sup> | Jiri Jäntti<sup>2,3</sup> | Juuso Tuppurainen<sup>2</sup> | Saskia Plomp<sup>1</sup> | Nikae Te Moller<sup>1</sup> | Janne T. A. Mäkelä<sup>2,3</sup> | Rene van Weeren<sup>1</sup> 

<sup>1</sup>Department of Equine Sciences, Utrecht University, Utrecht, The Netherlands

<sup>2</sup>Department of Applied Physics, University of Eastern Finland, Kuopio, Finland

<sup>3</sup>Clinical Physiology and Nuclear Medicine, Kuopio University Hospital, Kuopio, Finland

## Correspondence

Maria Fugazzola, Utrecht University, Department of Equine Sciences, Utrecht, The Netherlands.

Email: [m.c.fugazzola@uu.nl](mailto:m.c.fugazzola@uu.nl)

## Funding information

Instrumentarium Science Foundation, Academy of Finland, Grant/Award Number: 307932; Kuopio University Hospital, Grant/Award Number: 5041795

## Abstract

**Background:** Strategies for articular cartilage repair need to take into account topographical differences in tissue composition and architecture to achieve durable functional outcome. These have not yet been investigated in the equine stifle.

**Objectives:** To analyse the biochemical composition and architecture of three differently loaded areas of the equine stifle. We hypothesise that site differences correlate with the biomechanical characteristics of the cartilage.

**Study design:** Ex vivo study.

**Methods:** Thirty osteochondral plugs per location were harvested from the lateral trochlear ridge (LTR), the distal intertrochlear groove (DITG) and the medial femoral condyle (MFC). These underwent biochemical, biomechanical and structural analysis. A linear mixed model with location as a fixed factor and horse as a random factor was applied, followed by pair-wise comparisons of estimated means with false discovery rate correction, to test for differences between locations. Correlations between biochemical and biomechanical parameters were tested using Spearman's correlation coefficient.

**Results:** Glycosaminoglycan content was different between all sites (estimated mean [95% confidence interval (CI)] for LTR 75.4 [64.5, 88.2], for intercondylar notch (ICN) 37.3 [31.9, 43.6], for MFC 93.7 [80.1109.6]  $\mu\text{g}/\text{mg}$  dry weight), as were equilibrium modulus (LTR2.20 [1.96, 2.46], ICN0.48 [0.37, 0.6], MFC1.36 [1.17, 1.56] MPa), dynamic modulus (LTR7.33 [6.54, 8.17], ICN4.38 [3.77, 5.03], MFC5.62 [4.93, 6.36] MPa) and viscosity (LTR7.49 [6.76, 8.26], ICN16.99 [15.88, 18.14], MFC8.7 [7.91, 9.5] $^{\circ}$ ). The two weightbearing areas (LTR and MFC) and the non-weightbearing area (ICN) differed in collagen content (LTR 139 [127, 152], ICN176[162, 191], MFC 127[115, 139]  $\mu\text{g}/\text{mg}$  dry weight), parallelism index and angle of collagen fibres. The strongest correlations were between proteoglycan content and equilibrium modulus ( $r: 0.642$ ;  $p: 0.001$ ), dynamic modulus ( $r: 0.554$ ;  $p < 0.001$ ) and phase shift ( $r: -0.675$ ;

Maria Fugazzola and Mikko T. Nissinen shared first co-authorship.

This is an open access article under the terms of the [Creative Commons Attribution-NonCommercial](https://creativecommons.org/licenses/by-nc/4.0/) License, which permits use, distribution and reproduction in any medium, provided the original work is properly cited and is not used for commercial purposes.

© 2023 The Authors. *Equine Veterinary Journal* published by John Wiley & Sons Ltd on behalf of EVJ Ltd.

$p < 0.001$ ), and between collagen orientation angle and equilibrium modulus ( $r: -0.612$ ;  $p < 0.001$ ), dynamic modulus ( $r: -0.424$ ;  $p < 0.001$ ) and phase shift ( $r: 0.609$ ;  $p < 0.001$ ).

**Main limitations:** Only a single sample per location was analysed.

**Conclusions:** There were significant differences in cartilage biochemical composition, biomechanics and architecture between the three differently loaded sites. The biochemical and structural composition correlated with the mechanical characteristics. These differences need to be acknowledged by designing cartilage repair strategies.

#### KEYWORDS

cartilage ECM fibre orientation, collagen type II, proteoglycans, stiffness, topographical differences articular cartilage

## 1 | INTRODUCTION

Articular cartilage acquires its topographical heterogeneity in biomechanical characteristics during late gestation and early postnatal life.<sup>1,2</sup> The process mainly consists of a depth-dependent redistribution of biochemical components, such as glycosaminoglycans (GAGs) and collagen, with specific disposition and orientation or architecture, within the different layers of the tissue. This redistribution is highly dependent on the biomechanical forces to which the different areas are exposed after birth.<sup>3,4</sup> Early developmental changes and adaptation, as well as site-dependency of the biochemical, biomechanical and structural characteristics within the same joint have been studied in the equine fetlock.<sup>4–8</sup> The equine stifle has been less explored. Biochemical and biomechanical properties have been studied, but structural characteristics and constituent architecture of its articular cartilage have not been investigated so far.<sup>9,10</sup>

The relationship between structures, that is, the architecture and the biomechanical characteristics of articular cartilage have gained increasing interest in past years in the human field.<sup>11,12</sup> Since the architecture of the extracellular matrix of cartilage, together with its biochemical composition, determines the biomechanical properties of the tissue and is hence a crucial factor for its functionality, the topographical differences in native architecture within the joint become clinically relevant when considering cartilage repair. Strategies for cartilage regeneration or repair would need to take these differences into account in order to achieve a durable functional outcome.<sup>5,13</sup>

The stifle is a biomechanically versatile joint, with a unique loading pattern that includes impact, compression, tension and shear loading, and also contains non-weight-bearing areas. Being a high-mobility joint, focal articular cartilage damage, either caused by trauma or by the developmental orthopaedic disorder osteochondrosis dissecans (OCD), can cause lameness and may ultimately lead to osteoarthritis.<sup>14</sup> The most affected locations are the lateral trochlear ridge (LTR), in the form of OCD, and the medial femoral condyle, in which the development of subchondral cystic lesions is more frequent.<sup>15</sup> Mosaicplasty has been proposed as a therapeutic approach for the latter condition.<sup>16</sup> This autologous transplantation of an osteochondral block from

a non-weight-bearing area of the joint (the distal intertrochlear groove [DITG]/intercondular notch) to the damaged area, is also widely used in human orthopaedic surgery.<sup>17,18</sup> Considering how differently these two areas within the same joint are loaded, they can be expected to exhibit not only biomechanical and biochemical differences,<sup>9</sup> but also a different architecture.

The first aim of this study was to analyse three clinically relevant areas of the equine stifle that are subjected to different in-vivo loading patterns: the lateral femoral trochlea (subjected to mixed shear and impact forces through patella), the medial femoral condyle (MFC) (impact and shear forces through tibia) and the DITG (non-weight-bearing). We hypothesised that they would differ in their biochemical, biomechanical composition and also in their architecture, which would be reflected in the depth-dependent distribution of the structural components and collagen fibril orientation respectively. The second aim was to examine the relationships between these site-dependent biochemical and structural characteristics, and the principal biomechanical features of the articular cartilage.

## 2 | MATERIALS AND METHODS

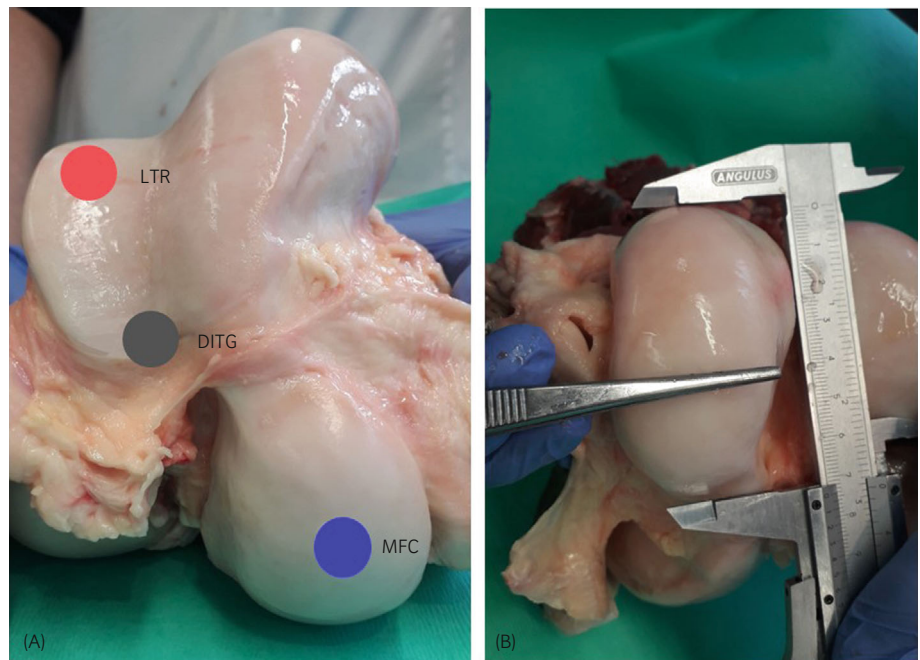
### 2.1 | Sample size estimates

Sample size estimates (using Wilcoxon signed ranks analysis of data) were performed using an online calculator<sup>19</sup> and based on previous studies.<sup>5,20</sup> With a power of 80% and alpha of 0.05, this yielded a sample size of 12–27, depending on the primary parameter (estimate mean differences in GAG and collagen content between two different sites of the fetlock joint) that was used to calculate the effect size. A conservative choice was made to collect 30 samples per location.

### 2.2 | Sampling procedure

Hindlimbs from livestock criollo horses between 4 and 6 years of age were harvested from an abattoir and stored frozen at  $-20^{\circ}\text{C}$ . On the

**FIGURE 1** The three sampling locations (A) DITG, distal intertrochlear groove; MFC, medial femoral condyle; LTR, lateral trochlear ridge. (B) Example of determining sampling location for the MFC (B).



day of the sample collection, after thawing, the joints were opened, the patella was removed, and the articular surfaces were examined for gross abnormalities. Any joints showing macroscopic abnormalities, including osteophytes, cartilage fibrillation or discolouring were excluded. Finally, 30 stifles were included in the study. From these, osteochondral plugs of 10 mm depth and 8.5 mm diameter were harvested using a hollow drill (Acufex<sup>®</sup>, Smith and Nephew), from three different locations within the joint (Figure 1A). Thirty osteochondral plugs were harvested from the MFC, the DITG and the LTR, respectively, making a total of 90 osteochondral plugs. The osteochondral plugs were labelled and stored at  $-80^{\circ}\text{C}$  until further processing.

For the medial condyle, the sampling location was chosen to represent the area sustaining the most biomechanical impact and compressive forces, based on published biomechanical studies of the equine stifle<sup>9,21,22</sup>: the transition point between the cranial and middle third of the cartilage-covered portion of the condyle on a longitudinal axis and in a central location on the transverse axis (Figure 1B). For the site on the LTR, which is subjected to mixed shear and impact forces through the patella, the location was defined as halfway between the proximal end of the trochlea and the synovial plica that separates the lateral femorotibial and femoropatellar joints, on the axial surface of the trochlea. The third sampling area was the non-weight-bearing DITG of the femur.

### 2.3 | Biochemical analysis

Cartilage derived from the border of the sampling area was used for DNA, GAG and hydroxyproline (HYP) quantification. Samples were digested overnight in papain solution, 500  $\mu\text{L}$  per sample (0.01 M cysteine, 250  $\mu\text{g}/\text{mL}$  papain, 0.2 M  $\text{NaH}_2\text{PO}_4$  and 0.01 M EDTA) at  $60^{\circ}\text{C}$ . Total DNA was quantified on the papain digest using the

Qubit 4.0 fluorimeter with the Qubit dsDNA BR Assay Kit (Q32853) according to the manufacturer's instructions. Total GAG content was determined by photospectrometry at 540 and 595 nm after reaction with dimethylmethylene blue using a microplate reader (Biorad). Collagen was quantified by using an HYP assay. Samples were freeze-dried and hydrolysed at  $108^{\circ}\text{C}$  overnight in 4 M NaOH. HYP was measured after reaction with Dimethylaminobenzaldehyde, the absorbance was read at 570 nm using a microplate reader (Clariostar<sup>®</sup>, BMG Labtech).

### 2.4 | Biomechanical analysis

After thawing at room temperature, thickness of the cartilage was analysed from micro-CT scans (Nikon XT H 225, Nikon Metrology Europe). The micro-CT scans were done to 2–5 plugs per scan. The plugs were in separate test tubes and a tube filled with water was used as a reference for the calculation of Hounsfield unit (HU) values. The scan reconstruction images were then exported to MATLAB, where a custom script was used to generate two-dimensional (2D) images and HU profiles for each sample individually. The sample thickness was determined as the distance from the surface to cartilage bone interface in pixels and the thickness in micrometres was calculated by multiplying the distance by pixel-size.

The biomechanical properties of the osteochondral plugs were determined in indentation geometry using a stress-relaxation protocol.<sup>23</sup> A custom-made measuring device was used that consisted of a displacement actuator with resolution of 0.1  $\mu\text{m}$  (PM1A11939, Newport) and a load cell of 0.25 kg (Model 31, Honeywell International Inc.). A goniometer was applied to ensure perpendicularity between the cartilage surface and the plane-ended cylindrical indenter (Figure 2). The diameter of the indenter was 0.55 mm. The osteochondral plugs were

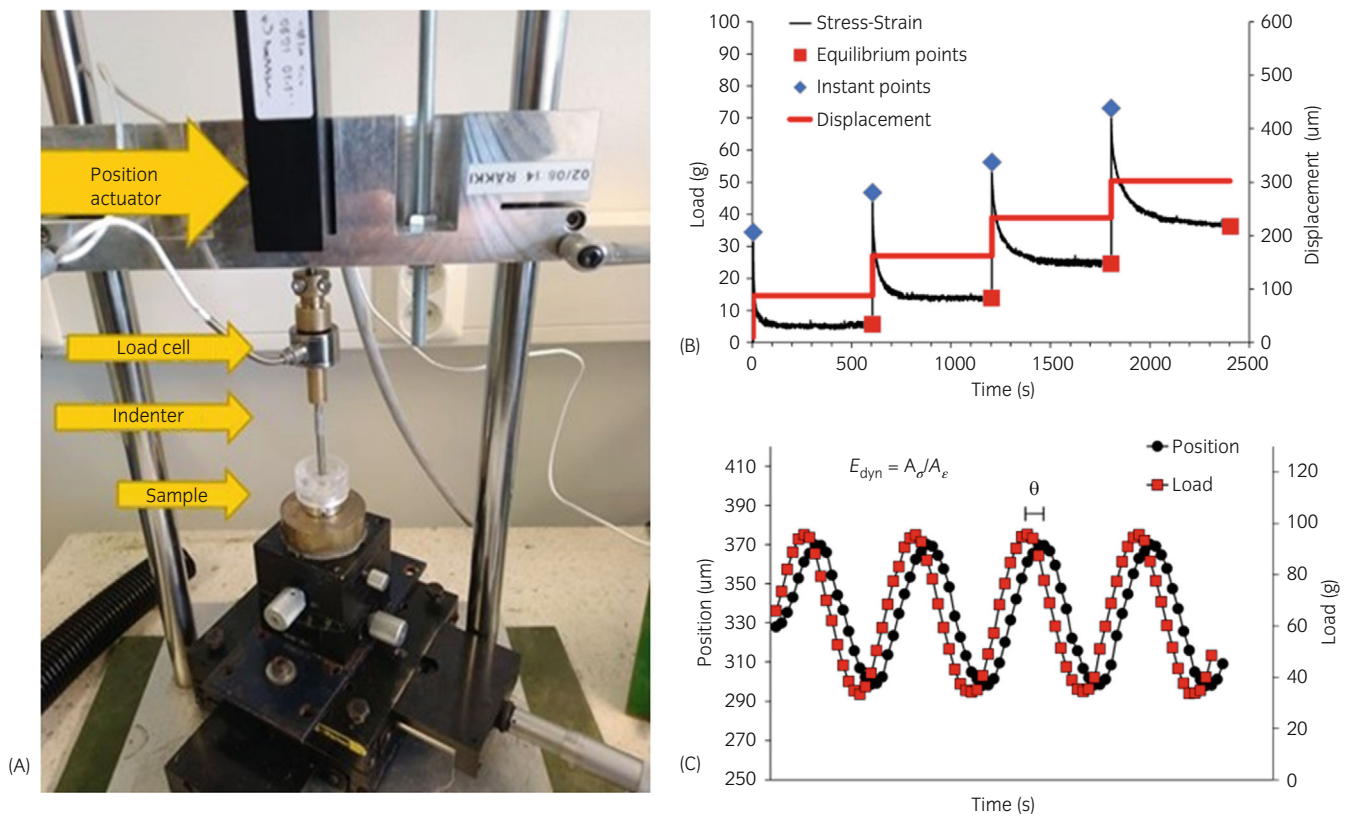


**FIGURE 2** (A) Custom-made mechanical indentation device with indenter of 0.55 mm diameter. (B) Graphical representation of the stress-relaxation protocol. The blue and red marks represent the points used for the calculation of the equilibrium and the instantaneous moduli. (C) Graphical representation of load and position curves. Before calculating the dynamic modulus, load was converted to stress and position to strain. The phase shift ( $\theta$ ) between the load and the position was analysed from a Fourier transform.

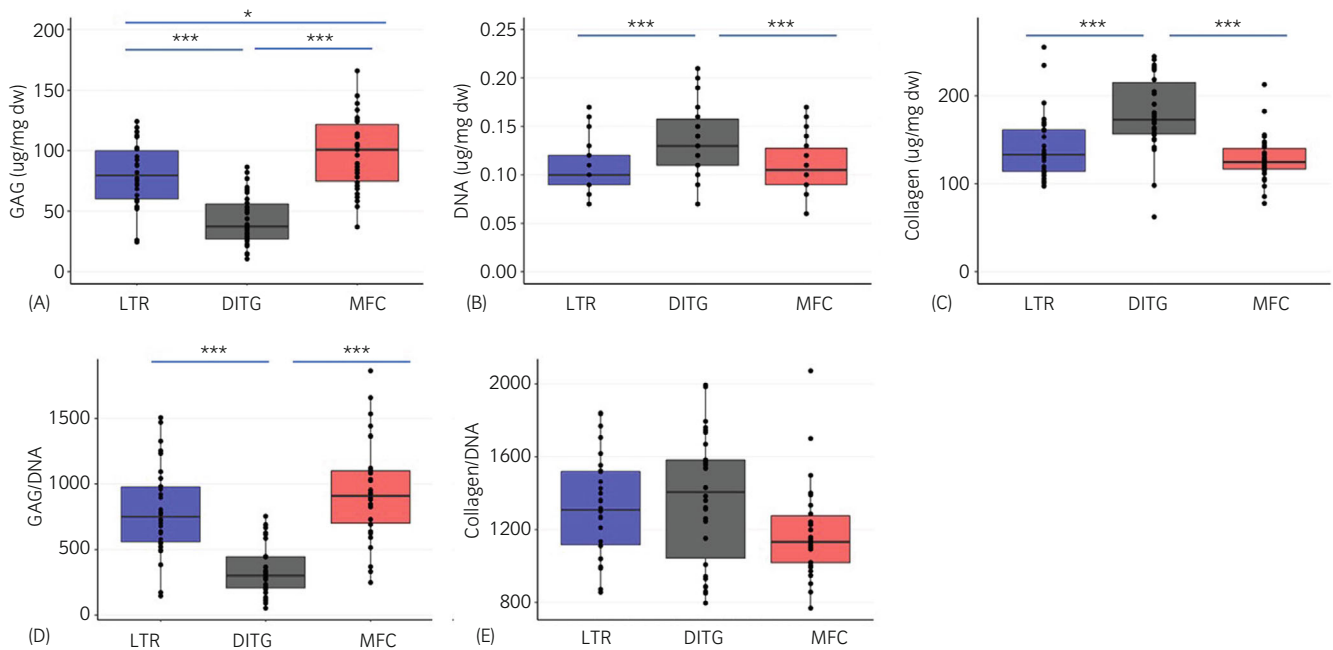


**FIGURE 3** Biochemical composition of articular cartilage in the three sampling locations. DITG, distal intertrochlear groove; LTR, lateral trochlear ridge; MFC, medial femoral condyle. Significant differences between the locations: \* $p < 0.05$ ; \*\* $p < 0.01$ ; \*\*\* $p < 0.001$ .



fixed at the bone with three screws to the bottom of a custom-made holder (an acrylic cup with a stainless-steel bottom) that was filled with PBS (phosphate-buffered saline, 310 mOsmol/L).

Full contact between the indenter and the cartilage surface was ensured with an equilibrium pre-stress of 40 kPa (1 g). Pre-strain remained below 2% for all samples from the first point of contact (recorded load). The testing protocol included four steps, each of them followed by 600 s relaxation time. Preliminary tests showed that the relaxation time of 600 s was long enough for the samples to reach equilibrium. A step size of 4% of the remaining cartilage thickness was utilised with a ramp rate of 100%/s (of the cartilage thickness). After the stress-relaxation protocol, without a lift-off, a sinusoidal dynamic test was implemented using 4% peak-to-peak strain amplitude of the remaining thickness, 4 cycles, and three different frequencies: 0.1, 0.5 and 1 Hz.

From the stress-relaxation protocol (Figure 3A), Young's equilibrium modulus ( $E_{Eq}$ ), the strain-dependent instantaneous modulus ( $E_E$ ) and the initial instantaneous modulus ( $E_0$ ) were determined.<sup>23</sup> The equilibrium and the instantaneous moduli were calculated by fitting a linear least-squares fit to the stress-strain measurement data.<sup>24</sup> The dynamic modulus ( $E_{dyn}$ ) was determined from the sinusoidal test, from the ratio of the stress and strain amplitudes (Figure 3B), and a phase shift ( $\theta$ ) was analysed from a Fourier transform. To account for the indentation geometry effect on the results, the Hayes correction was utilised.<sup>24</sup>

## 2.5 | Structural analysis

After fixation in formalin, and histologic preparation, the samples were processed for depth-dependent microscopic and spectroscopic analysis of tissue composition and structure.

Proteoglycan (PG) content and distribution were determined with digital densitometry (DD) from Safranin O-stained sections using a CCD camera (SenSys, Photometrics Inc.) mounted on a light microscope (Leitz Orthoplan, Leitz).<sup>25</sup> Greyscale images of the sections were captured and converted into optical density. Optical density was determined quantitatively in a depth-wise manner.

The collagen content was estimated with Fourier transform infrared (FTIR) spectroscopy (A Perkin Elmer Spotlight 300, Perkin Elmer) using the integrated absorbance of the amide I region (Wavelength: 1585–1720  $\text{cm}^{-1}$ ).<sup>26,27</sup>

Polarised light microscopy (PLM) (Leitz Ortholux II POL, Leitz) was used to analyse the collagen orientation angles ( $0^\circ$  indicating an angle parallel to the cartilage surface and  $90^\circ$  indicating an angle perpendicular to the cartilage surface) and to determine the parallelism index of the collagen fibrils, based on Stokes parameters.<sup>28</sup> The collagen fibril orientation angle in the samples was measured in a depth-dependent manner using a Leitz Ortholux II POL polarised light microscope (Leitz Wetzlar), a CCD camera (Photometrics Inc.), a monochromatic light source, and polarisers. For DD, FTIR and PLM analysis, three sections were measured from each sample using a 4 $\times$  magnification objective and averaged.

## 2.6 | Statistical methods

RStudio (version 2021.09.2, RStudio, PBC) and Matlab (version R2020b, Mathworks) were used for the statistics. A linear mixed model (lme4 package, version 1.1-27.1) with location as a fixed factor and horse as a random factor was used, followed by pair-wise comparisons of estimated means with false discovery rate correction, to test for differences between locations. For the depth-dependent analysis with DD and FTIR, each measurement was analysed in 1% steps from cartilage surface to calcified cartilage. The measured value at each depth was considered as the dependent variable, while the effect of the site and horse were fixed and random variables, respectively. Square root transformation of data was used for the biomechanical data and the collagen content, while log transformation was applied to GAG data. Correlations between biochemical and biomechanical parameters were tested using Spearman's correlation coefficient. Statistical significance was set at  $p < 0.05$ .

## 3 | RESULTS

### 3.1 | Biochemical analysis

GAG content was significantly different among all sites (Figure 4A). The estimated mean of GAG content was highest for MFC (estimate mean [95% confidence interval (CI)] 93.7 [80.1, 109.6]  $\mu\text{g}/\text{mg}$  dry weight), which was significantly different from LTR (estimate mean [95% CI] 75.4 [64.5, 88.2]  $\mu\text{g}/\text{mg}$  dry weight;  $p < 0.05$ ) and from intercondylar notch (ICN) (estimate mean [95% CI] 37.3 [31.9, 43.6]  $\mu\text{g}/\text{mg}$  dry weight;  $p < 0.0001$ ). DNA content was highest for ICN (estimate mean [95% CI] 0.136 [0.125, 0.147]  $\mu\text{g}/\text{mg}$  dry weight), which was significantly higher compared to LTR (estimate mean [95% CI] 0.109 [0.098, 0.120]  $\mu\text{g}/\text{mg}$  dry weight;  $p < 0.001$ ), and compared to MFC (estimate mean [95% CI] 0.112 [0.101, 0.123]  $\mu\text{g}/\text{mg}$  dry weight;  $p < 0.001$ ). The latter two were not significantly different (Figure 4B). Collagen content was highest in ICN (estimate mean [95% CI] 176 [162, 191]  $\mu\text{g}/\text{mg}$  dry weight) and was significantly different compared to LTR (estimate mean [95% CI] 139 [127, 152]  $\mu\text{g}/\text{mg}$  dry weight;  $p < 0.001$ ) and MFC (estimate mean [95% CI] 127 [115, 139]  $\mu\text{g}/\text{mg}$  dry weight;  $p < 0.0001$ ). Here too, LTR and MFC were not significantly different (Figure 4C). When corrected for cellularity, GAG-levels were significantly lower in the ICN compared to the other two locations, but collagen/DNA did not differ significantly between the three sites (Figures 4D,E).

### 3.2 | Biomechanical analysis

The equilibrium modulus ( $E_{eq}$ ) and dynamic modulus ( $E_{dyn}$ ) were significantly different among all sites (Figure 5). The estimated mean  $E_{eq}$  in LTR (estimate mean [95% CI] 2.2 [1.96, 2.45] MPa) was significantly and substantially higher compared to ICN (estimate mean [95% CI] 0.48 [0.37, 0.60] MPa;  $p < 0.001$ ) and to MFC (estimate mean [95% CI] 1.36 [1.17, 1.56] MPa;  $p < 0.001$ ). LTR also had a higher initial instantaneous modulus ( $E_0$ ) (estimate mean [95% CI] 3.64 [3.07,

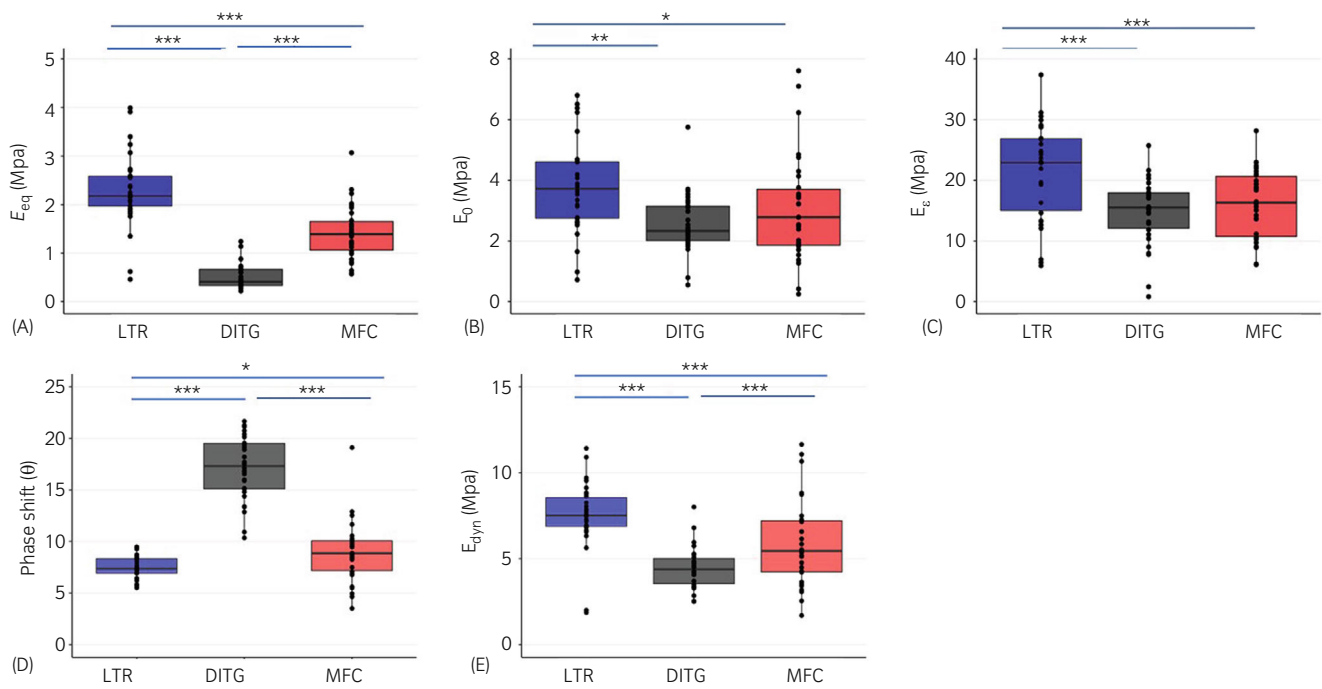


**FIGURE 4** Biomechanical properties of articular cartilage in the three sampling locations. DITG, distal intertrochlear groove; LTR, lateral trochlear ridge; MFC, medial femoral condyle;  $E_{eq}$ , equilibrium modulus (A);  $E_0$ , initial instantaneous modulus (B);  $E_s$ , strain-dependent instantaneous modulus (C);  $\theta$ , phase shift (D)  $E_{dyn}$ , dynamic modulus (E). Significant differences between the locations: \* $p < 0.05$ ; \*\* $p < 0.01$ ; \*\*\* $p < 0.001$ .

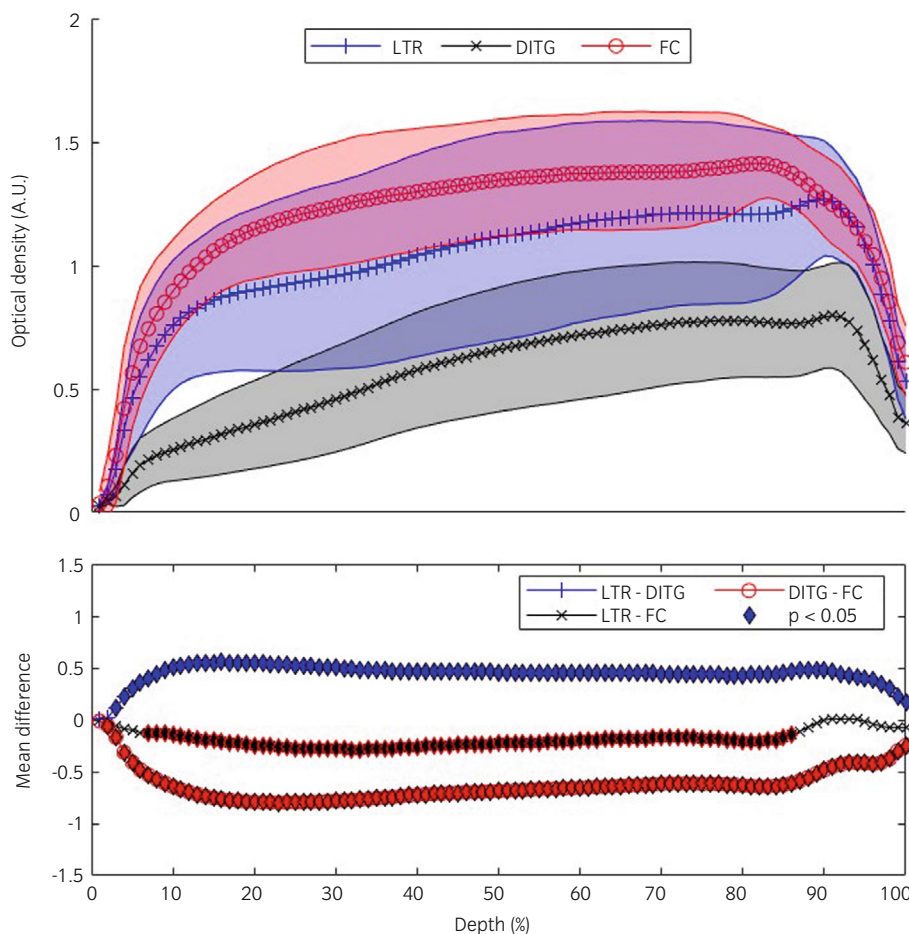


**FIGURE 5** Graphical representation of the PG distribution, defined from digital densitometry images, of the three locations and the difference between them, in a depth-dependent manner (0 surface, 100 cartilage-bone interface). The depicted profiles indicate the mean value of each location (full line with markers) and the standard deviation (shaded areas). The mean difference between each pair is indicated with a marker and the significant differences ( $p < 0.05$ ) are noted with a triangle. DITG, distal intertrochlear groove; LTR, lateral trochlear ridge; MFC, medial femoral condyle.

4.25] MPa) compared to locations ICN (estimate mean [95% CI] 2.46 [2.00, 2.97] MPa;  $p < 0.01$ ) and MFC (estimate mean [95% CI] 2.82 [2.32, 3.36] MPa;  $p < 0.05$ ). The strain-dependent instantaneous modulus ( $E_e$ ) followed a comparable pattern. Phase shift was significantly higher in the ICN (estimate mean [95% CI] 16.99 [15.88, 18.14] $^\circ$ ) compared to LTR (estimate mean [95% CI] 7.49 [6.76, 8.26] degrees;  $p < 0.001$ ) and MFC (estimate mean [95% CI] 8.7 [7.91, 9.5] $^\circ$ ;  $p < 0.001$ ).

### 3.3 | DD: Depth-dependent proteoglycan distribution

Proteoglycan content was significantly different ( $p < 0.05$ ) between all three locations, through the whole normalised thickness of the samples (Figure 6), with MFC showing the highest content, followed by LTR and ICN. The profiles indicated lower levels of PGs in the most superficial layers and increasing PG content in the middle and deep layers for all the samples.

### 3.4 | Spectroscopy: Depth-dependent collagen distribution

Collagen content distribution among sites was significantly different ( $p < 0.05$ ) between ICN and MFC, and between ICN and LTR, in the

superficial and middle layers of the samples (Figure 7). Collagen content in MFC and LTR differed significantly in the superficial and deep zone. Note that the small peaks in density just below the surface seen in LTR and MFC are missing in ICN.

### 3.5 | Polarised light microscopy: Depth-dependent fibril orientation angle and parallelism index

In the superficial layer, the orientation angle of collagen fibrils was lower, that is, more parallel to the articular surface in all sites, compared to the middle and deep layers. However, the ICN showed a much less sharp change in orientation angle with a gradual change from 0 to 90 $^\circ$ , resulting in a thicker transitional zone compared to LTR and MFC (Figures 8 and 9).

In line with the above, the parallelism index of the collagen fibrils was significantly different ( $p < 0.05$ ) between ICN and LTR, and between ICN and MFC in the superficial zone and in the middle zone, where also the difference between MFC and LTR was significant. The change in degree of parallelism as a function of depth is more abrupt (hence, taking place over a shorter distance) in LTR and MFC. In the ICN, this change is more gradual and takes place over a considerably longer distance.

Representative images of DD, spectroscopy and polarised light microscopy of the three analysed locations are shown in Figure 9.

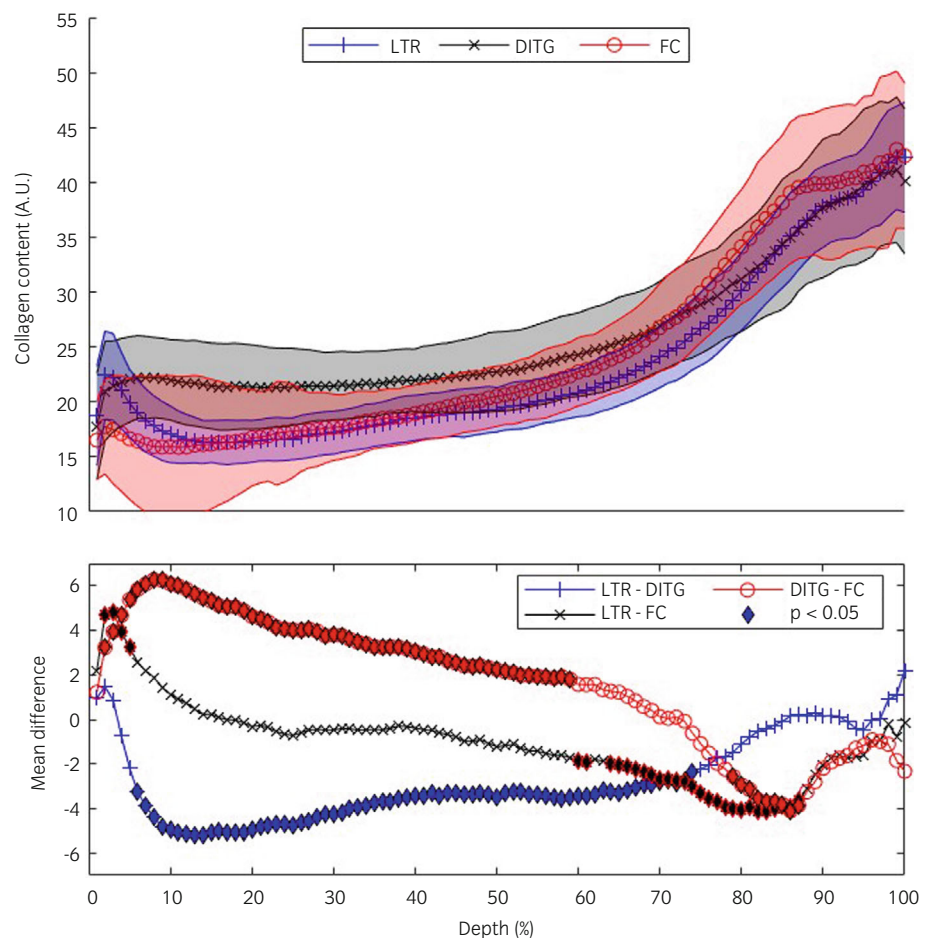


**FIGURE 6** Graphical representation of the collagen distribution, defined from FTIR images of the three locations and the mean difference between them, in a depth-dependent manner (0 surface, 100 cartilage-bone interface). The depicted profiles indicate the mean value of each location (full line with markers) and the standard deviation (shaded areas). The mean difference between each pair is indicated with a marker and the significant differences ( $p < 0.05$ ) are noted with a triangle. AU, arbitrary unit; DITG, distal intertrochlear groove; LTR, lateral trochlear ridge; MFC, medial femoral condyle.

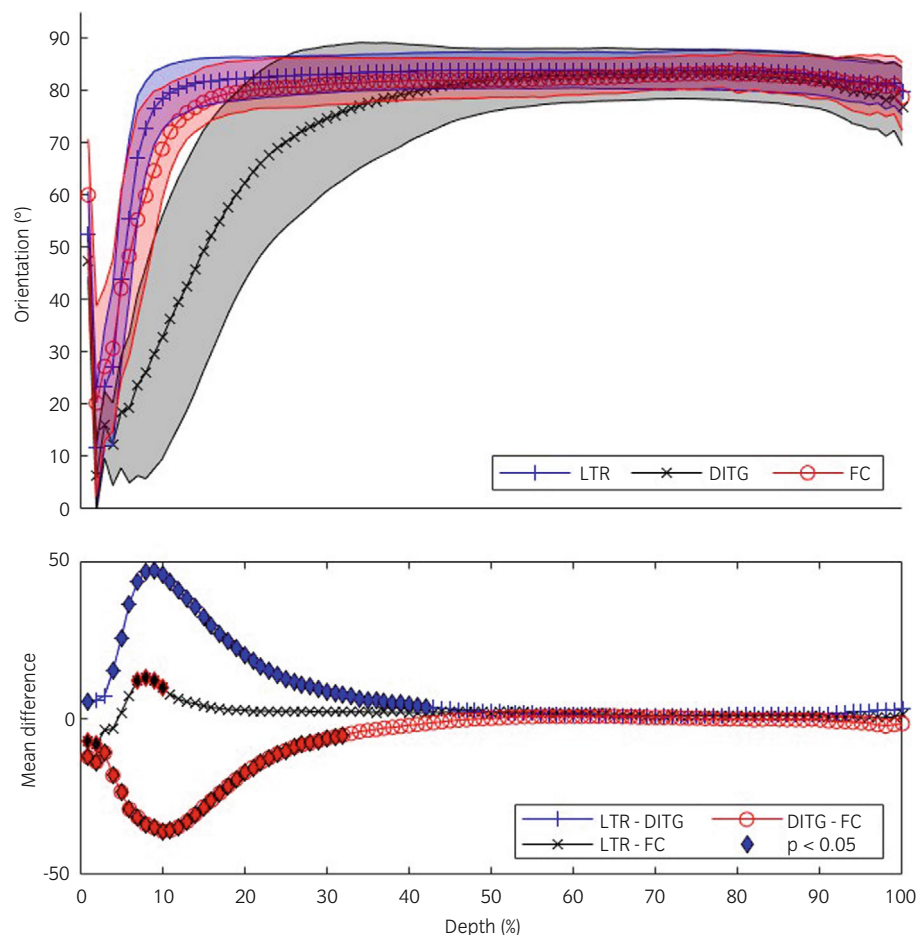


**FIGURE 7** Graphical representation of the collagen fibril orientation angle defined from PLM images of the three locations and the mean difference between them, represented in a depth-dependent manner (0 surface, 100 cartilage-bone interface). The depicted profiles indicate the mean value of each location (full line with markers) and the standard deviation (shaded areas). The mean difference between each pair is indicated with a marker and the significant differences ( $p < 0.05$ ) are noted with a triangle. DITG, distal intertrochlear groove; LTR, lateral trochlear ridge; MFC, medial femoral condyle.

### 3.6 | Correlation analysis

#### 3.6.1 | Biochemistry versus biomechanics

A positive significant correlation was observed between GAG content and  $E_{eq}$ ,  $E_0$  and  $E_{dyn}$  (Table 1) and between collagen content and phase shift. A negative significant correlation was observed between GAG content and phase shift and between collagen content and  $E_{eq}$  and  $E_{dyn}$ .

#### 3.6.2 | Depth-dependent collagen and PG distribution, fibril orientation angle and parallelism index with biomechanical proprieties

PG content, defined from DD, had a positive correlation with  $E_e$  and the other elastic moduli and a negative correlation with phase shift (Table 2). Also, collagen content showed a positive correlation with  $E_e$  and phase shift. Collagen orientation angle correlated negatively with  $E_{eq}$ ,  $E_e$ , and  $E_{dyn}$ , and positively with  $\theta$ . The parallelism index correlated significantly with phase shift.

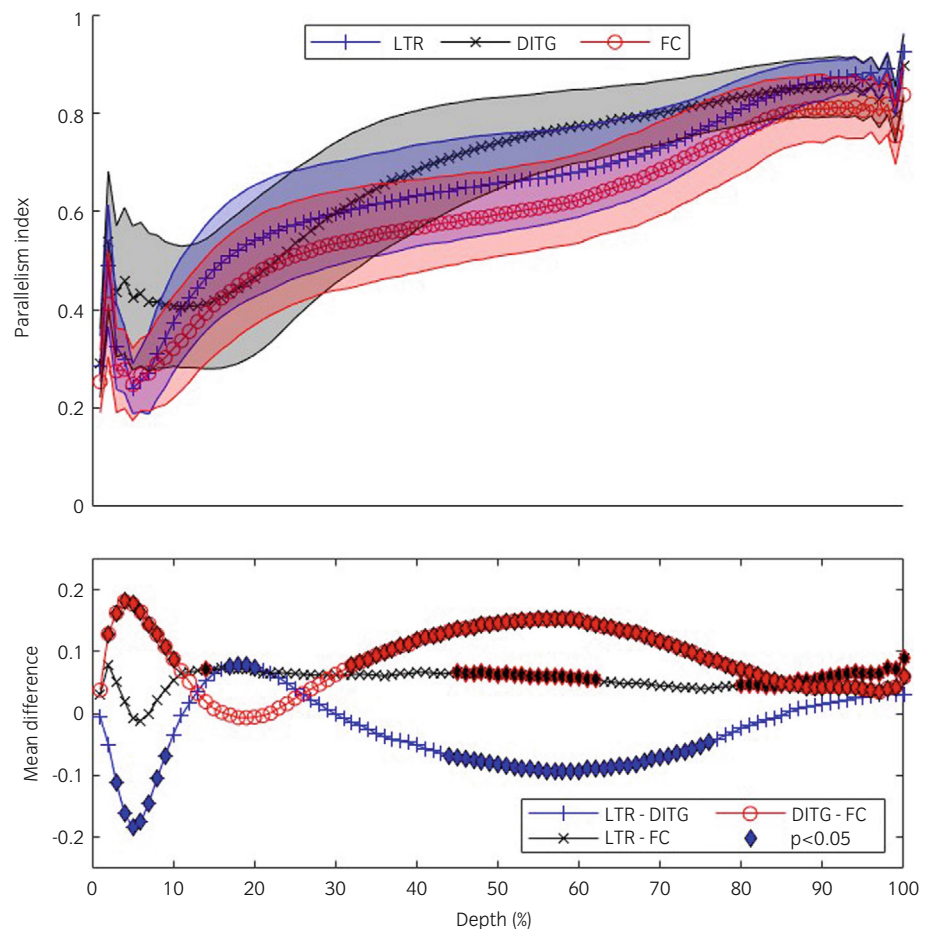
## 4 | DISCUSSION

These results show that biomechanical properties, composition and architecture of equine articular cartilage have significant site-to-site variation within the stifle joint, strongly suggesting an adaptation to the local mechanical loading environment. The LTR is subjected to mixed shear and compressive forces during motion, generated by the sliding over it of the lateral aspect of the patella, but also to mere compression when the horse is standing on the limb with the patella in a locked position. The distal intertrochlear groove experiences short-lasting transient contact with the patella during flexion but is to a large extent a non-weight-bearing area. The femoral condyle is constantly subjected to compressive forces while the horse is standing and experiences mixed compressive and shear forces during locomotion.<sup>22</sup>

The largest differences occurred between the weight-bearing and non-weight-bearing areas. LTR and MFC exhibited the highest GAG content, which correlated with the equilibrium modulus. This higher stiffness in the LTR and MFC, that experience the highest compressive forces, is biologically logical. The finding is also in line with corroborated knowledge, that at equilibrium, once the fluid has ceased



**FIGURE 8** Graphical representation of the collagen fibril parallelism index defined from PLM images of the three locations and the difference between them, in a depth-dependent manner (0 surface, 100 cartilage-bone interface). The depicted profiles indicate the mean value of samples (full line with markers) and the standard deviation (shaded areas). The mean difference between each pair is indicated with a marker and the significant differences ( $p < 0.05$ ) are noted with a triangle. DITG, distal intertrochlear groove; LTR, lateral trochlear ridge; MFC, medial femoral condyle.



flowing out of the tissue, GAGs are mainly responsible for the tissue's compressive stiffness.<sup>29</sup> Furthermore, earlier studies in both young and mature horses have shown that healthy cartilage responds to increased loading through exercise programs by producing more GAGs with collagen levels remaining stable, hence, increasing the relative GAG content of the extracellular matrix, which observations underline the interplay between loading and largely GAG-determined stiffness of the cartilage.<sup>30,31</sup> The high correlation between GAG content and equilibrium modulus found in our study ( $r = 0.60$ ) is close to the one reported by Changoor et al. ( $r = 0.71$ ) in a study comparing biochemical and biomechanical characteristics of articular cartilage, and subchondral bone in the equine stifle, in a larger number of locations but using a smaller study population.<sup>9</sup> Similar to our results, in that study the MFC also contained the highest amount of GAGs.

In our study, collagen content was higher in the less loaded area of the ICN when compared to the two loaded areas of MFC and LTR. This concurs with a study where cartilage from two locations within the fetlock joint was compared between foals undergoing a training program (i.e., more loading) and foals being raised at pasture (i.e., less loading).<sup>32</sup> The cartilage of the trained group showed less collagen content than the non-trained group, while the number of crosslinks in

the trained animals was higher in the loaded areas. The lower collagen content in higher loaded areas, as found in our study and the one cited above, suggests that there is a re-distribution of collagen from a 'default situation' at birth that takes place in the early postnatal phase and is mostly based on loading. In that sense, the non-weight-bearing trochlear notch analysed in the present study can be considered to be closer to the prenatal 'default' stage of cartilage structure than in the loaded sites. Comparable rearrangements during the development of components exposed to different amounts of loading can be seen also in other tissues of the locomotion apparatus. The bone mineral density of the metacarpal and sesamoid bones in foals was significantly higher in box-rested foals compared to those subjected to training.<sup>33,34</sup> Similarly, the collagen content in the tendons of foals receiving box rest was higher than those being exercised, but the number of crosslinks was higher in the tendons of the exercised group.<sup>35</sup>

As an engineering material, articular cartilage is commonly described as fibril-reinforced poroviscoelastic, and the behaviour of the tissue consists of fluid flow-dependent and flow-independent mechanisms. Viscoelasticity is a key characteristic of cartilage function and the current results show big differences in the viscoelasticity between the sites. In addition to being the softest site, ICN was seen to exhibit highly viscous behaviour (Figure 5D) compared to the more

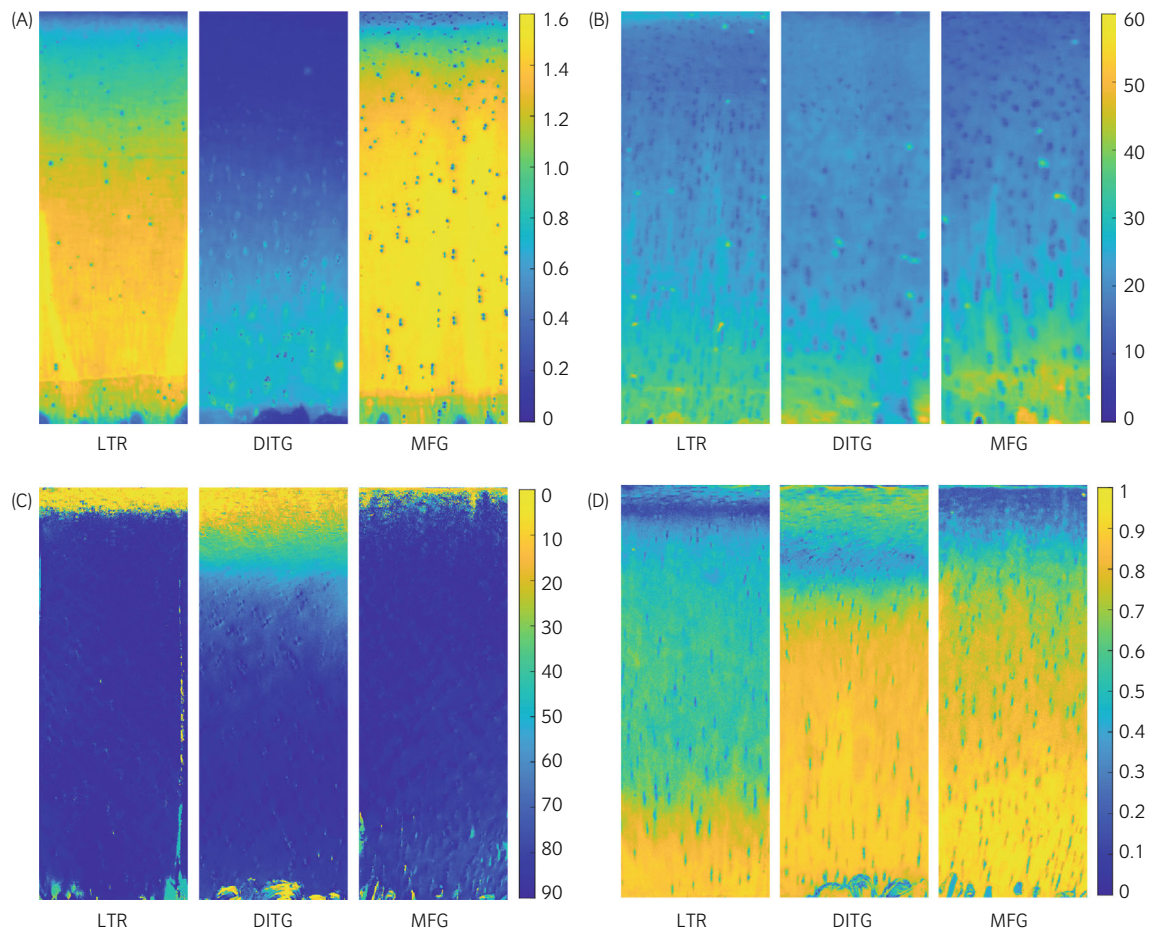


**FIGURE 9** Representative examples of full-thickness cartilage sections from LTR, DITG and MFC represented in the different imaging modalities. In all images, the articular surface is at the top of the image and subchondral bone is located at the bottom. (A) Digital densitometry image for depth-dependent determination of the proteoglycan distribution: The colour scale indicates the amount of proteoglycans with yellow containing the highest amount and blue containing the least amount. The scale numbers are arbitrary units. (B) Spectroscopy image for depth-dependent determination of the collagen distribution: The colour scale indicates the amount of collagen content with yellow containing the highest amount and blue containing the least amount. The scale numbers are arbitrary units. (C) Polarised light images for determination of the collagen fibril orientation: The colour scale indicates the angle of the collagen fibres with yellow showing orientation parallel to the surface ( $0^\circ$ ) and dark blue orientation perpendicular to the surface ( $90^\circ$ ). (D) Polarised light images for determination of the collagen fibril parallelity index: The colour scale indicates the parallelism index (PI) of the collagen fibres with yellow showing parallel orientation of the fibres (PI 1) and dark blue random orientation towards each other (PI 0).

**TABLE 1** Correlations between biochemical and biomechanical variables

	$E_{eq}$ $r$	$E_e$ $r$	$E_0$ $r$	$(\theta)$ $r$	$E_{dyn}$ $r$
GAG	0.596***	0.273**	0.421***	-0.584***	0.524***
Coll	-0.462***	-0.354**	-0.218*	0.527***	-0.392***

Abbreviations:  $E_{dyn}$ , dynamic modulus;  $E_{eq}$ , equilibrium modulus;  $E_e$ , strain-dependent instantaneous;  $E_0$ , initial instantaneous modulus;  $r$ , Spearman correlation coefficient;  $\theta$ , phase shift.

\* $p < 0.05$ ; \*\* $p < 0.01$ ; \*\*\* $p < 0.001$ .

elastic LTR and MFC regions (which had a lower phase shift). Based on the current correlation analysis and past results, PGs, with their capability to bind water, increase the cartilage elasticity (Tables 1 and 2)<sup>36</sup> and allow the tissue to withstand compressive forces.

Simultaneously, collagen fibres and their architecture increase the viscosity.<sup>36</sup> The viscous and inertial losses in the continuum are critical to load resistance and dissipation, and were more pronounced in the ICN tissue that undergoes mainly sliding motion of the patella.

**TABLE 2** Correlations between structural and biomechanical features of the cartilage.

	$E_{eq}$ $r$	$E_e$ $r$	$E_0$ $r$	$(\theta)$ $r$	$E_{dyn}$ $r$
PG content (DD)	<b>0.642***</b>	<b>0.417***</b>	<b>0.270**</b>	<b>-0.675***</b>	<b>0.554***</b>
Collagen content (FTIR)	<b>-0.326**</b>	-0.156	-0.057	<b>0.489***</b>	-0.196
Collagen orientation angle (PLM)	<b>-0.612***</b>	<b>-0.235*</b>	-0.188	<b>0.609***</b>	<b>-0.424***</b>
Parallelism index (PLM)	-0.126	-0.105	-0.032***	<b>0.285**</b>	-0.089

Note: Angle, orientation angle of collagen fibrils. Significant correlations are in bold.

Abbreviations: DD, digital densitometry = PG content;  $E_{dyn}$ , dynamic modulus;  $E_{eq}$ , equilibrium modulus;  $E_e$ , strain-dependent instantaneous modulus;  $E_0$ , initial instantaneous modulus;  $(\theta)$ , phase shift; FTIR, Fourier transform infrared spectroscopy intensity = collagen content; PI, parallelism index of collagen fibrils;  $r$ , spearman correlation coefficient.

\* $p < 0.05$ ; \*\* $p < 0.01$ ; \*\*\* $p < 0.001$ .

With respect to the collagen architectural arrangement of the sampled sites, the findings closely followed the observations of the biochemical composition and a strong correlation was observed between the collagen orientation angle and the related parallelism index, and mechanics. Overall, the cartilage function is seen to be more influenced by the architecture and arrangement of the collagen network, rather than the absolute amount of the structural protein, being in line with the previous studies.<sup>37</sup> There were only minor differences in the architecture of LTR and MFC. At both sites, there were short transitional zones in which the predominant orientation angle changed from 0° (parallel to the articular surface) to 90° (perpendicular to that surface) and consequently a small zone with a low parallelism index. In an architectural sense, this translates as the Benninghoff arcades having long pillars and a relatively low arch. Resulting in a relatively large deep zone, which is known to have the greatest resistance against compressive forces.<sup>38</sup> The situation in the ICN was different with a much thicker transitional area, a consequently larger area with a low parallelism area and also a relatively thinner deep zone, in accordance with the lower GAG-content and compressive stiffness of the tissue.

The current results emphasise the importance of the intricate architecture and interplay between cartilage structure and function. Other reports on the relation between the structure of cartilage and its biomechanics in the horse and other species, including humans, are in line with our results.<sup>8,12,39,40</sup> Still, studies on equine cartilage repair techniques commonly evaluate the quality of the obtained repair tissue by means of histological and biochemical analyses only failing to test the repair tissue structurally and even more important functionally, that is, biomechanically.<sup>13</sup> Our findings once more stress the important relationship between loading and biomechanical functionality of articular cartilage and how this is achieved by nature through site-dependent adaptations in both composition and architecture of the tissue. Therefore, biomechanical evaluation of repair cartilage within experimental research appears not only an important asset, but in fact a *conditio sine qua non* for a proper functional evaluation.

On a clinical level, the site-dependent differences are of interest when considering the cartilage properties of donor sites for the repair of osteochondral defects. Subchondral bone cysts, for example, are a

commonly encountered osteochondral disease in the horse, often communicating with the articular surface of the medial femoral condyle. Mosaicplasty, involving harvesting osteochondral plugs from a non-weight-bearing area of the joint and implanting them into the defective area, is one of the proposed therapies. In an experimental study, in sound horses in which plugs were harvested from the medial femoral trochlear ridge and implanted in the contralateral medial femoral condyle, in 50% of the horses these plugs had kept their native hyaline cartilage cover at 9–12 months follow-up, in the other 50% the tissue changed to hyaline-like cartilage or fibrocartilage.<sup>17</sup> In humans, mosaicplasty has been used more extensively with positive clinical long-term outcomes, but the results vary greatly depending on age, sex, and size of the lesion.<sup>41</sup> Allografts consisting of donor cartilage from the exact same location needing repair would contain similar characteristics to the recipient site, since the cartilage has been ‘trained’ for a similar biomechanical environment during maturation. However, with allografting, there are challenges with tissue availability and the possibility of an immunologic response by the recipient remains.<sup>42,43</sup> With the advancement of cartilage repair strategies, such as three-dimensional bio-printing, it would seem a logical path to specifically adapt constructs to the local biomechanical environment they will be implanted into.

A limitation of the current study is that a single site per biomechanical region was analysed. The variation between samples from the same site was low, so we are confident that we were able to sample in a consistent way, but the investigated characteristics might alter if the sampling location had been more proximal or distal within the same region. In a recent study in which three sites were analysed within the same region, significant biochemical differences could not be found but the aggregate modulus showed differences between sites, as was the case with the study by Changoor et al.<sup>7,10</sup> Since our aim was to characterise areas with a specific in-vivo loading pattern and to compare these areas, extensive mapping of the regions was not performed.

In conclusion, elaborate variances in the biomechanical properties between three differently loaded sites of the adult equine stifle joint are reported for the first time. These differences are related to the biochemical composition and the architecture of the extracellular matrix of the cartilage. Having implications for practice, and guiding

directions for future allotransplantation, the results show for instance how collagen matrix architecture (fibril orientation) alters cartilage biomechanics more than the bulk amount of the protein. Given the fact that the mechanical functionality is the key characteristics of articular cartilage, rather than qualitative histology and biochemical measurements alone, biomechanics should be the main benchmark for judging the (potential) performance of constructs or other regenerative techniques for defect repair at given sites of the joint.

#### AUTHOR CONTRIBUTIONS

Maria Fugazzola helped conceive the study, performed the research including data interpretation and wrote the manuscript. Mikko T. Nissinen contributed with the methods of biomechanical analysis and with data analysis and critically reviewed the manuscript. Jiri Jäntti performed the micro CT measurements, helped with data analysis and critically reviewed the manuscript. Juuso Tuppurainen contributed with the biomechanical analysis and critically reviewed the manuscript. Saskia Plomp contributed with the biochemical analysis and critically reviewed the manuscript. Nikae Te Moller contributed with data analysis and critically reviewed the manuscript, Janne T. A. Mäkelä contributed to conceiving the study, data interpretation and critically reviewed the manuscript. Rene van Weeren conceived the study, helped with data interpretation and critically reviewed the manuscript.

#### ACKNOWLEDGEMENTS

Instrumentarium Science Foundation, Academy of Finland (project number 307932), Kuopio University Hospital (VTR grant number 5041795).

#### CONFLICT OF INTEREST STATEMENT

The authors declare no conflict of interest.

#### PEER REVIEW

The peer review history for this article is available at <https://www.webofscience.com/api/gateway/wos/peer-review/10.1111/evj.13960>.

#### DATA AVAILABILITY STATEMENT

The data that support the findings of this study are available from the corresponding author upon reasonable request.

#### ETHICAL ANIMAL RESEARCH

Research ethics committee oversight not currently required by this journal: the study was performed on material obtained from an abattoir.

#### INFORMED CONSENT

Not applicable.

#### ORCID

Maria Fugazzola  <https://orcid.org/0000-0002-4152-0948>

Rene van Weeren  <https://orcid.org/0000-0002-6654-1817>

#### REFERENCES

1. Van Turnhout MC, Schipper H, Engel B, Buist W, Kranenburg S, Van Leeuwen JL. Postnatal development of collagen structure in ovine articular cartilage. *BMC Dev Biol.* 2010;10:60. <https://doi.org/10.1186/1471-213X-10-62>
2. Van Turnhout MC, Kranenburg S, Van Leeuwen JL. Contribution of postnatal collagen reorientation to depth-dependent mechanical properties of articular cartilage. *Biomech Model Mechanobiol.* 2011; 10(2):269–79. <https://doi.org/10.1007/S10237-010-0233-7>
3. Julkunen P, Halmesmäki EP, Iivarinen J, Rieppo L, Närhi T, Marjanen J, et al. Effects of growth and exercise on composition, structural maturation and appearance of osteoarthritis in articular cartilage of hamsters. *J Anat.* 2010;217(3):262–74. <https://doi.org/10.1111/j.1469-7580.2010.01270.x>
4. Brama PAJ, Tekoppele JM, Bank RA, Barneveld A, van Weeren PR. Development of biochemical heterogeneity of articular cartilage: influences of age and exercise. *Equine Vet J.* 2002;34(3):265–9. <https://doi.org/10.2746/042516402776186146>
5. Brama PAJ, Tekoppele JM, Bank RA, Karsenberg D, Barneveld A, van Weeren PR. Topographical mapping of biochemical properties of articular cartilage in the equine fetlock joint. *Equine Vet J.* 2000; 32(1):19–26. <https://doi.org/10.2746/042516400777612062>
6. Oinas J, Ronkainen AP, Rieppo L, Finnilä MAJ, Iivarinen JT, van Weeren PR, et al. Composition, structure and tensile biomechanical properties of equine articular cartilage during growth and maturation. *Sci Rep.* 2018;8(1):11357. <https://doi.org/10.1038/s41598-018-29655-5>
7. Hyttinen MM, Holopainen J, van Weeren PR, Firth EC, Helminen HJ, Brama PAJ. Changes in collagen fibril network organization and proteoglycan distribution in equine articular cartilage during maturation and growth. *J Anat.* 2009;215(5):584–91. <https://doi.org/10.1111/j.1469-7580.2009.01140.x>
8. Julkunen P, Harjula T, Iivarinen J, Marjanen J, Seppänen K, Närhi T, et al. Biomechanical, biochemical and structural correlations in immature and mature rabbit articular cartilage. *Osteoarthr Cartil.* 2009; 17(12):1628–38. <https://doi.org/10.1016/j.joca.2009.07.002>
9. Changoor A, Hurtig MB, Runciman RJ, Quesnel AJ, Dickey JP, Lowerison M. Mapping of donor and recipient site properties for osteochondral graft reconstruction of subchondral cystic lesions in the equine stifle joint. *Equine Vet J.* 2006;38(4):330–6. <https://doi.org/10.2746/042516406777749254>
10. White JL, Salinas EY, Link JM, Hu JC, Athanasiou KA. Characterization of adult and neonatal articular cartilage from the equine stifle. *J Equine Vet Sci.* 2021;96:103294. <https://doi.org/10.1016/j.jevs.2020.103294>
11. Mäkelä JTA, Rezaeian ZS, Mikkonen S, Madden R, Han S-K, Jurvelin JS, et al. Site-dependent changes in structure and function of lapine articular cartilage 4 weeks after anterior cruciate ligament transection. *Osteoarthr Cartil.* 2014;22(6):869–78. <https://doi.org/10.1016/j.joca.2014.04.010>
12. Mäkelä JTA, Huttu MRJ, Korhonen RK. Structure-function relationships in osteoarthritic human hip joint articular cartilage. *Osteoarthr Cartil.* 2012;20(11):1268–77. <https://doi.org/10.1016/J.JOCA.2012.07.016>
13. Fugazzola MC, van Weeren PR. Surgical osteochondral defect repair in the horse—a matter of form or function? *Equine Vet J.* 2020;52(4): 489–99. <https://doi.org/10.1111/evj.13231>
14. Barrett M, Frisbie D. Stifle. In: McLlwrath CW, Frisbie D, Kawcak C, Goodrich L, van Weeren R, editors. *Joint disease in the horse*. 2nd ed. St. Louis, Missouri: Elsevier; 2016. p. 385.
15. Fowlie J G, Stick J, Nickels F. The stifle. *Equine Surgery*. 4th ed. Missouri: Elsevier S. St Louis; 2012. p. 1435–6.
16. Bodó G, Vásárhelyi G, Hangody L, Módos L. Mosaic arthroplasty of the medial femoral condyle in horses — an experimental study. *Acta Vet Hung.* 2013;62(2):155–68. <https://doi.org/10.1556/avet.2013.059>



17. Martín AR, Patel JM, Zlotnick HM, Carey JL, Mauck RL. Emerging therapies for cartilage regeneration in currently excluded 'red knee' populations. *NPJ Reg Med.* 2019;4(1):1–11. <https://doi.org/10.1038/S41536-019-0074-7>
18. Medvedeva EV, Grebenik EA, Gornostaeva SN, Telpuhov VI, Lychagin AV, Timashev PS, et al. Repair of damaged articular cartilage: current approaches and future directions. *Int J Mol Sci.* 2018;19(8):2366. <https://doi.org/10.3390/IJMS19082366>
19. Ristler R. Sample size Calculator Version 1.0541. 2021 <https://homepage.univie.ac.at/robin.ristl/samplesize.php?test=wilcoxon>
20. Brama PAJ, Holopainen J, van Weeren PR, Firth EC, Helminen HJ, Hyttinen MM. Effect of loading on the organization of the collagen fibril network in juvenile equine articular cartilage. *J Orthop Res.* 2009;27(9):1226–34. <https://doi.org/10.1002/jor.20866>
21. Halley SE, Bey MJ, Haladik JA, Lavagnino M, Arnoczky SP. Three dimensional, radiostereometric analysis (RSA) of equine stifle kinematics and articular surface contact: a cadaveric study. *Equine Vet J.* 2014;46(3):364–9. <https://doi.org/10.1111/evj.12127>
22. Fowlie JG, Arnoczky SP, Stick JA, Pease AP. Meniscal translocation and deformation throughout the range of motion of the equine stifle joint: an in vitro cadaveric study. *Equine Vet J.* 2011;43(3):259–64. <https://doi.org/10.1111/j.2042-3306.2010.00291.x>
23. Huttu MRJ, Puhakka J, Mäkelä JTA, Takakubo Y, Tiitu V, Saarakkala S, et al. Cell-tissue interactions in osteoarthritic human hip joint articular cartilage. *Connect Tissue Res.* 2014;55(4):282–91. <https://doi.org/10.3109/03008207.2014.912645>
24. Hayes WC, Keer LM, Herrmann G, Mockros LF. A mathematical analysis for indentation tests of articular cartilage. *J Biomech.* 1972;5(5):541–51. [https://doi.org/10.1016/0021-9290\(72\)90010-3](https://doi.org/10.1016/0021-9290(72)90010-3)
25. Kiviranta I, Jurvelin J, Säämänen AM, Helminen HJ. Microspectrophotometric quantitation of glycosaminoglycans in articular cartilage sections stained with safranin O. *Histochemistry.* 1985;82(3):249–55. <https://doi.org/10.1007/BF00501401>
26. Boskey A, Pleshko CN. FT-IR imaging of native and tissue-engineered bone and cartilage. *Biomaterials.* 2007;28(15):2465–78. <https://doi.org/10.1016/J.BIOMATERIALS.2006.11.043>
27. Camacho N, West P, Torzilli P, Mendelsohn R. FTIR microscopic imaging of collagen and proteoglycan in bovine cartilage. *Biopolymers.* 2001;62:1–8. [https://doi.org/10.1002/1097-0282\(2001\)62:1%3C1::AID-BIP10%3E3.0.CO;2-O](https://doi.org/10.1002/1097-0282(2001)62:1%3C1::AID-BIP10%3E3.0.CO;2-O)
28. Rieppo J, Hyttinen MM, Halmesmaki E, Ruotsalainen H, Vasara A, Kiviranta I, et al. Changes in spatial collagen content and collagen network architecture in porcine articular cartilage during growth and maturation. *Osteoarthr Cartil.* 2009;17(4):448–55. <https://doi.org/10.1016/j.joca.2008.09.004>
29. Mansour JM. *Biomechanics of cartilage. Kinesiology: The Mechanics and Pathomechanics of Human Movement.* 2nd ed. Philadelphia, PA: Lippincott Williams & Wilkins; 2013. p. 69–83.
30. Murray RC, Birch HL, Lakhani K, Goodship AE. Biochemical composition of equine carpal articular cartilage is influenced by short-term exercise in a site-specific manner. *Osteoarthr Cartil.* 2001;9(7):625–32. <https://doi.org/10.1053/JOCA.2001.0462>
31. Brama PA, Tekoppele JM, Bank RA, van Weeren PR, Barneveld A. Influence of different exercise levels and age on the biochemical characteristics of immature equine articular cartilage. *Equine Vet J.* 1999;31(S31):55–61. <https://doi.org/10.1111/J.2042-3306.1999.TB05314.X>
32. van Weeren PR, Firth EC, Brommer H, Hyttinen MM, Helminen AE, Rogers CW, et al. Early exercise advances the maturation of glycosaminoglycans and collagen in the extracellular matrix of articular cartilage in the horse. *Equine Vet J.* 2008;40(2):128–35. <https://doi.org/10.2746/042516408X253091>
33. Cornelissen BP, van Weeren PR, Ederveen AG, Barneveld A. Influence of exercise on bone mineral density of immature cortical and trabecular bone of the equine metacarpus and proximal sesamoid bone. *Equine Vet J.* 1999;31(S31):79–85. <https://doi.org/10.1111/J.2042-3306.1999.TB05318.X>
34. Stover SM, Pool RR, Martin RB, Morgan JP. Histological features of the dorsal cortex of the third metacarpal bone mid-diaphysis during postnatal growth in thoroughbred horses. *J Anat.* 1992;181(Pt 3):455.
35. Cherdchutham W, Becker C, Smith RK, Barneveld A, van Weeren PR. Age-related changes and effect of exercise on the molecular composition of immature equine superficial digital flexor tendons. *Equine Vet J.* 1999;31(S31):86–94. <https://doi.org/10.1111/J.2042-3306.1999.TB05319.X>
36. Ebrahimi M, Turunen MJ, Finnilä MA, Joukainen A, Kröger H, Saarakkala S, et al. Structure–function relationships of healthy and osteoarthritic human Tibial cartilage: experimental and numerical investigation. *Ann Biomed Eng.* 2020;48(12):2887–900. <https://doi.org/10.1007/S10439-020-02559-0>
37. Broom ND. Abnormal softening in articular cartilage. Its relationship to the collagen framework. *Arthritis Rheum.* 1982;25(10):1209–16. <https://doi.org/10.1002/ART.1780251010>
38. Eschweiler J, Horn N, Rath B, Betsch M, Baroncini A, Tingart M, et al. The biomechanics of cartilage—an overview. *Life.* 2021;11(4):1647–57. <https://doi.org/10.3390/LIFE11040302>
39. Nelson BB, Mäkelä JTA, Lawson TB, Patwa AN, Barrett MF, McIlwraith CW, et al. Evaluation of equine articular cartilage degeneration after mechanical impact injury using cationic contrast-enhanced computed tomography. *Osteoarthr Cartil.* 2019;27(8):1219–28. <https://doi.org/10.1016/j.joca.2019.04.015>
40. Nelson BB, Makela JTA, Lawson TB, Patwa AN, Snyder BD, McIlwraith CW, et al. Cationic contrast-enhanced computed tomography distinguishes between reparative, degenerative, and healthy equine articular cartilage. *J Orthop Res.* 2020;39(8):1647–57. <https://doi.org/10.1002/jor.24894>
41. Nakagawa Y, Mukai S, Yabumoto H, Tarumi E, Nakamura T. Serial changes of the cartilage in recipient sites and their Mirror sites on second-look imaging after Mosaicplasty. *Am J Sports Med.* 2016;44(5):1243–8. <https://doi.org/10.1177/0363546516634299>
42. De Caro F, Bisicchia S, Amendola A, Ding L. Large fresh osteochondral allografts of the knee: a systematic clinical and basic science review of the literature. *Arthroscopy.* 2015;31(4):757–65. <https://doi.org/10.1016/J.ARTHRO.2014.11.025>
43. Sherman SL, Garrity J, Bauer K, Cook J, Stannard J, Bugbee W. Fresh osteochondral allograft transplantation for the knee: current concepts. *J Am Acad Orthopaed Surg.* 2014;22(2):121–33. <https://doi.org/10.5435/JAAOS-22-02-121>

**How to cite this article:** Fugazzola M, Nissinen MT, Jäntti J, Tuppurainen J, Plomp S, Te Moller N, et al. Composition, architecture and biomechanical properties of articular cartilage in differently loaded areas of the equine stifle. *Equine Vet J.* 2024;56(3):573–85. <https://doi.org/10.1111/evj.13960>